Journal of Holography Applications in Physics
Volume 6, Issue 1, Winter 2026, 82–97
©Available online at http://jhap.du.ac.ir
DOI: 10.22128/jhap.2025.2988.1132
Online ISSN: 2783–3518

Regular article

Holographic Dark Energy Models and Late Time Cosmic Acceleration in Light of Recent Observations

Sonali Borah
Department of Physics, Assam University, Silchar-788011,Assam, India;
E-mail: sonalicosmo@gmail.com

Received: August 26, 2025; **Revised:** November 17, 2025; **Accepted:** November 18, 2025

Abstract. Holographic dark energy (HDE) models, based on the holographic principle, offer a quantum gravity-inspired explanation for the Universe's late-time acceleration. In HDE models, the vacuum energy density relates to an infrared (IR) cutoff, determined by horizon scales. In this study, we performed parameter estimation using the latest observational data, including Type Ia Supernovae, GRBs and observed Hubble parameters across various holographic dark energy models. We employ the Markov Chain Monte Carlo (MCMC) method to evaluate the viability of these models. Our results show that holographic dark energy models are consistent with existing data and provide insights into the dynamic nature of dark energy. This research highlights the deep connection between cosmological observations and quantum gravity concepts to enhance our understanding of cosmic acceleration.

Keywords: Cosmic Aceleration; Dark Energy; Holographic Principle; IR Cutoff.

Contents

1 Introduction

The detection of the Universe's accelerated expansion in the late 20th century [1,2] profoundly transformed modern cosmology. Independent confirmations from cosmic microwave background (CMB) anisotropies [3], baryon acoustic oscillations (BAO) [4], and cosmic chronometer (CC) measurements [5] have firmly validated cosmic acceleration as an essential observational reality. Within the standard cosmological framework, this phenomenon is attributed to a cosmological constant Λ. In the Λ cold dark matter (ΛCDM) model, which continues to provide an excellent fit to most datasets [3,6]. Nevertheless, the ΛCDM model faces theoretical challenges, especially the cosmological constant issue [7,8] and the coincidence problem, which drive the investigation of alternative explanations for dark energy (DE).

The holographic principle, first proposed by 't Hooft [9] and later developed by Susskind [10], posits that all physical information contained within a spatial region can be encoded on its boundary surface. When applied to cosmology, this concept constrains the vacuum energy such that the total energy enclosed within a cosmological horizon does not exceed that of a black hole of the same scale [8,11]. Consequently, the dark energy density becomes associated with an infrared (IR) cutoff, and the specific choice of this cutoff gives rise to different holographic dark energy models.

In the standard Holographic Dark Energy (HDE) scenario, the IR cutoff is identified with the future event horizon, allowing the resulting energy density to reproduce the observed late-time acceleration of the Universe [11]. The Ricci Dark Energy (RDE) model offers an alternative interpretation by associating the cutoff with the Ricci scalar curvature, $L^{-2} \propto R$, thereby linking dark energy to the local spacetime geometry and reducing the inherent nonlocality of the original HDE formulation [12].

In contrast, the New Agegraphic Dark Energy (NADE) model relates the IR cutoff to the *conformal time* of the Universe $\eta = \int_0^t \frac{dt'}{a(t')}$, which encapsulates the cumulative causal structure of cosmic evolution. This leads to a dark energy density of the form $\rho_{\mathrm{NADE}} = 3n^2 M_p^2/\eta^2$ [13], thereby connecting spacetime quantum fluctuations with large-scale cosmic dynamics.

A further generalization, termed Barrow Holographic Dark Energy (BHDE), modifies the entropy area relation by introducing a deformation parameter Δ that incorporates possible quantum gravitational corrections and fractal aspects of spacetime [14]. Together, the RDE, NADE, and BHDE models provide complementary realizations of the holographic principle, each characterized by a distinct physical choice of the IR cutoff, either through curvature, causal structure, or horizon deformation. Collectively, these frameworks highlight how information bounds and quantum effects may influence the evolution of dark energy and the late-time expansion of the Universe.

Prominent variants include the Ricci Dark Energy (RDE) model [12,15], which employs the Ricci scalar as the IR cutoff and thereby avoids the non-locality of the event horizon; the New Agegraphic Dark Energy (NADE) model [13,16], in which the conformal age of the Universe sets the cutoff, motivated by spacetime quantum fluctuations; and the more recent Barrow Holographic Dark Energy (BHDE) model [14,17], which incorporates Barrow entropy, a quantum-gravitational deformation of the Bekenstein–Hawking entropy, introducing a new parameter Δ that modifies the dark energy density scaling. These models have been studied in various cosmological contexts, from background expansion to structure formation [18]. With the rise of precise observational sets like the Pantheon Type Ia supernova catalog [6], refined CC estimates [19], and gamma-ray burst (GRB) relations [20–22], one can now constrain holographic dark energy scenarios with remarkable accuracy. In

this study,we conduct a comparative investigation of BHDE, RDE and NADE employing SN Ia, CC and GRB observations.Through the use of statistical tools including the Akaike Information Criterion (AIC) and the Bayesian Information Criterion (BIC), we evaluated their comparative effectiveness and plausibility as substitutes for ΛCDM in describing the late-time cosmic acceleration.

Unlike earlier studies that used limited or low redshift data combinations like SNe Ia + CC or SNe Ia + CMB + BAO to constrain the Barrow, Ricci, and New Age graphic holographic dark energy models [11,18,23], the current analysis uses a fully geometric and model independent dataset made up of cosmic chronometers (CC), Type Ia supernovae, and gamma ray bursts (GRBs).This joint dataset spans a broad redshift range ($0 < z \lesssim 9$) and avoids early universe assumptions tied to the sound horizon. CC data provide direct measurements of the Hubble parameter $H(z)$ through galaxy age differentials [24], the SNe Ia sample minimizes calibration and systematic uncertainties [25], and the inclusion of GRBs extends the redshift reach to $z \sim 6$–9 [21,22]. Together, these complementary probes with joint datasets span both low and high redshift regimes, allowing for a comprehensive late-time assessment of holographic dark energy models, leading to tighter and more robust constraints on Ω_{m0}, H_0, and the model specific parameters compared to earlier analyses. In the next section, we build upon these theoretical foundations to formulate the cosmological dynamics of each model and examine their observational consistency using current datasets.

The structure of this paper is as follows. Section 2 provides a brief overview of the holographic dark energy models under consideration. Section 3 describes the observational datasets, analysis techniques, and the statistical model selection criteria employed. The cosmological constraints and their implications are presented in section 4. Finally, section 5 summarizes our findings and offers concluding remarks.

2 Holographic Dark Energy Models

2.1 Ricci Holographic Dark Energy (RDE)

The dark-energy density is proportional to the Ricci scalar of the FRW background [12,15]:

$$\rho_{\rm RDE} = 3\alpha M_p^2 \left(2H^2 + \dot{H}\right), \tag{2.1}$$

where α is a dimensionless parameter to be constrained by data.

The first Friedmann equation with matter ($\rho_m = \rho_{m0} a^{-3}$) and RDE reads

$$3M_p^2 H^2 = \rho_{m0} a^{-3} + 3\alpha M_p^2 \left(2H^2 + \dot{H}\right). \tag{2.2}$$

Divide by $3M_p^2 H_0^2$ and define $r \equiv E^2$ to obtain

$$(1 - 2\alpha) r - \alpha \frac{\dot{H}}{H_0^2} = \Omega_{m0} a^{-3}. \tag{2.3}$$

Using $x \equiv \ln a$ and $\frac{dr}{dx} = 2\dot{H}/H_0^2$ (since $d(H^2)/dx = 2\dot{H}$),

$$\frac{dr}{dx} - \left(\frac{2}{\alpha} - 4\right) r = -\frac{2}{\alpha}\, \Omega_{m0}\, a^{-3}. \tag{2.4}$$

This is a first-order linear ODE with solution

$$E^2(z) = \frac{2}{2-\alpha}\, \Omega_{m0} (1+z)^3 + \left[1 - \frac{2}{2-\alpha}\, \Omega_{m0}\right] (1+z)^{\,4-\frac{2}{\alpha}}. \tag{2.5}$$

Imposing $E(0) = 1$ fixes the integration constant. Equation (2.5) matches the standard analytic solution (see, e.g., Eq. (32) in [15]). For $\alpha \to 0$ one recovers ΛCDM-like behavior with an early-time $(1+z)^4$ component; observational fits typically require $0 < \alpha < 1$ [12,15].

2.2 Barrow Holographic Dark Energy (BHDE)

Barrow entropy modifies the Bekenstein–Hawking entropy to $S_B \propto A^{1+\Delta/2}$ with $0 \leq \Delta \leq 1$ [14]. Applying the holographic principle with Barrow entropy leads to the BHDE density [17,18]:

$$\rho_{\rm BHDE} = C\, L^{\,\Delta-2}, \tag{2.6}$$

where C has dimensions $[L]^{-2-\Delta}$ and L is the IR cutoff. The original and most used choice in BHDE is the future event horizon R_h,

$$R_h \equiv a\int_t^\infty \frac{dt'}{a(t')} = a\int_a^\infty \frac{da'}{Ha'^2}, \tag{2.7}$$

yielding $\rho_{\rm BHDE} = C\, R_h^{\Delta-2}$ [18].

Define $\Omega_{\rm B} \equiv \rho_{\rm BHDE}/(3M_p^2H^2)$. For $0 \leq \Delta < 1$ one obtains the autonomous equation for $\Omega_{\rm B}(x)$ [18]:

$$\frac{\Omega_{\rm B}'}{\Omega_{\rm B}(1-\Omega_{\rm B})} = 1 + \Delta + Q\,(1-\Omega_{\rm B})^{\frac{\Delta}{2(\Delta-2)}}\,\Omega_{\rm B}^{\frac{1}{2-\Delta}}\,e^{\frac{3\Delta}{2(\Delta-2)}x}, \tag{2.8}$$

with

$$Q = (2-\Delta)\left(\frac{C}{3M_p^2}\right)^{\frac{1}{\Delta-2}}\left(H_0\sqrt{\Omega_{m0}}\right)^{\frac{\Delta}{2-\Delta}}. \tag{2.9}$$

The BHDE equation of state is [18]

$$w_{\rm B} = -\frac{1+\Delta}{3} - \frac{Q}{3}\,\Omega_{\rm B}^{\frac{1}{2-\Delta}}(1-\Omega_{\rm B})^{\frac{\Delta}{2(\Delta-2)}}\,e^{\frac{3\Delta}{2(2-\Delta)}x}. \tag{2.10}$$

Once (2.8) is integrated from $z = 0$ (with $\Omega_{\rm B0} = 1-\Omega_{m0}$), the Hubble function follows from the flatness relation

$$E^2(z) = \frac{\Omega_{m0}(1+z)^3}{1-\Omega_{\rm B}(z)}. \tag{2.11}$$

If one instead chooses $L = H^{-1}$, then $\rho_{\rm BHDE} = 3c^2M_p^2H^{2-\Delta}$ and the Friedmann equation gives an algebraic relation

$$E^2(z) = \Omega_{m0}(1+z)^3 + \beta\,E^{2-\Delta}(z), \qquad \beta \equiv c^2\,H_0^{-\Delta}, \tag{2.12}$$

which can be solved analytically only for special Δ (e.g. $\Delta = 0, 1$) and otherwise is obtained numerically. See [17] for model details; most observational analyses adopt the event-horizon form (2.6)–(2.11).

2.3 New Agegraphic Dark Energy (NADE)

In NADE the IR cutoff is the conformal time η [13]:

$$\rho_{\rm NADE} = \frac{3n^2M_p^2}{\eta^2}, \qquad \eta \equiv \int_0^t \frac{dt'}{a(t')} = \int_0^a \frac{da'}{a'^2H(a')}, \tag{2.13}$$

where n is a dimensionless parameter of order unity. Defining $\Omega_{\rm q} \equiv \rho_{\rm NADE}/(3M_p^2H^2) = n^2/(H^2\eta^2)$ one has the useful identity

$$H\eta = \frac{n}{\sqrt{\Omega_{\rm q}}}\,. \tag{2.14}$$

The NADE equation of state in a flat universe reads,

$$w_{\rm q} = -1 + \frac{2}{3an}\sqrt{\Omega_{\rm q}}\,. \tag{2.15}$$

Using the conservation equations with dust matter, the general relation $\Omega'_{\rm de} = -3w_{\rm de}\,\Omega_{\rm de}(1-\Omega_{\rm de})$ yields the NADE evolution

$$\Omega'_{\rm q} = \Omega_{\rm q}(1-\Omega_{\rm q})\left[3 - \frac{2}{an}\sqrt{\Omega_{\rm q}}\right]. \tag{2.16}$$

Equivalently, in redshift form (using $d/dz = -(1+z)^{-1}d/d\ln a$ and $a = 1/(1+z)$),[8]

$$\frac{d\Omega_{\rm q}}{dz} = -\frac{\Omega_{\rm q}(1-\Omega_{\rm q})}{1+z}\left[3 - \frac{2(1+z)}{n}\sqrt{\Omega_{\rm q}}\right]. \tag{2.17}$$

After solving (2.16) (or (2.17)) with initial condition $\Omega_{\rm q0} = 1 - \Omega_{m0}$, one obtains

$$E^2(z) = \frac{\Omega_{m0}(1+z)^3}{1-\Omega_{\rm q}(z)}. \tag{2.18}$$

This is the standard way $H(z)$ is built in NADE studies [13].

3 Methodology

3.1 Data Analysis

In this work we constrain the model parameters θ of the dark-energy models using three complementary data-sets: cosmic chronometers (CC) $H(z)$ measurements, the Pantheon Type Ia supernova compilation, and a calibrated gamma-ray burst (GRB) Hubble diagram. Below we summarize the data and the statistical treatment used in the likelihood analysis.

Cosmic chronometers (CC)

The CC (differential age) measurements provide direct, model-independent estimates of the Hubble parameter $H(z)$ through the relative ages of passively evolving galaxies [19]. We use the latest compilations of CC measurements in the redshift range $0 \lesssim z \lesssim 2$ (see reviews and compilations in [19]). The theoretical prediction for each measurement is

$$H_{\rm th}(z_i;\theta,H_0) = H_0\,E(z_i;\theta), \tag{3.1}$$

where $E(z) \equiv H(z)/H_0$ is given by the model. The χ^2 for the CC dataset is computed as a simple sum over datapoints:

$$\chi^2_{\rm CC}(\theta,H_0) = \sum_{i=1}^{N_{\rm CC}} \frac{\left[H_{\rm obs}(z_i) - H_{\rm th}(z_i;\theta,H_0)\right]^2}{\sigma^2_{H,i}}. \tag{3.2}$$

If desired, H_0 can be treated as a free parameter in the global fit or marginalized over with a Gaussian prior; in many analyses a uniform prior on H_0 or an external prior (e.g. from Riess et al.) is used. The CC data are independent of the supernova absolute magnitude nuisance parameter and therefore help break degeneracies with H_0 [19].

Pantheon SNe Ia sample

We adopt the Pantheon compilation of SNe Ia as our primary low-redshift distance probe [25]. For a spatially-flat universe the Hubble-free luminosity distance is

$$D_L(z;\theta) = (1+z)\int_0^z \frac{dz'}{E(z';\theta)}, \tag{3.3}$$

and the theoretical distance modulus is

$$\mu_{\rm th}(z;\theta,\mathcal{M}) = 5\log_{10} D_L(z;\theta) + \mathcal{M}, \tag{3.4}$$

where $\mathcal{M} \equiv M_B + 5\log_{10}\left(\frac{c/H_0}{\rm Mpc}\right) + 25$ absorbs the absolute magnitude M_B and the Hubble constant. The Pantheon likelihood uses the full covariance matrix (statistical plus systematic) provided by the authors. Denoting the vector of observed distance moduli as $\boldsymbol{\mu}_{\rm obs}$ and the model vector as $\boldsymbol{\mu}_{\rm th}(\theta,\mathcal{M})$, the χ^2 reads

$$\chi^2_{\rm SN}(\theta,\mathcal{M}) = \Delta\boldsymbol{\mu}^T\,\mathbf{C}^{-1}\,\Delta\boldsymbol{\mu}, \qquad \Delta\boldsymbol{\mu} \equiv \boldsymbol{\mu}_{\rm obs} - \boldsymbol{\mu}_{\rm th}(\theta,\mathcal{M}), \tag{3.5}$$

where $\mathbf{C}$ is the Pantheon covariance matrix [25]. Following standard practice one can analytically marginalize over the nuisance parameter $\mathcal{M}$ (equivalently over M_B and H_0 combination) assuming a flat prior. The marginalized χ^2 is obtained by expanding Eq. (3.5) in $\mathcal{M}$ and minimizing, analogous to the treatment of μ_0 in older SN compilations.

Gamma-Ray Bursts (GRBs)

Long-duration GRBs extend the Hubble diagram to much higher redshifts than SNe Ia, and can therefore provide extra leverage on the expansion history when properly calibrated. A commonly used approach is a cosmology-independent calibration of GRB luminosity (or energy) correlations (for example the Amati relation $E_{p,i}$–$E_{\rm iso}$ or other empirical relations) by anchoring to the low-redshift SNe Ia Hubble diagram [20–22]. In this work we adopt a calibrated GRB Hubble diagram constructed via a model-independent interpolation of the Pantheon SNe Ia (see [20–22] for details), which produces a set of GRB distance moduli $\mu_{\rm GRB}(z_i)$ with uncertainties $\sigma_{\mu,{\rm GRB},i}$. The χ^2 contribution from GRBs is then

$$\chi^2_{\rm GRB}(\theta) = \sum_{i=1}^{N_{\rm GRB}} \frac{\left[\mu_{\rm GRB,obs}(z_i) - \mu_{\rm th}(z_i;\theta,\mathcal{M})\right]^2}{\sigma^2_{\mu,i}}, \tag{3.6}$$

where $\mu_{\rm th}$ uses the same $\mathcal{M}$ definition as for SNe Ia. When the GRB calibration was performed cosmology-independently (by interpolation on SNe), the calibration removes explicit cosmology dependence; however, residual systematic uncertainties should be propagated into $\sigma_{\mu,i}$ or accounted for via an extra systematic covariance term [22].

The combined likelihood is given by

$$\mathcal{L}_{\rm tot} \propto \exp\!\left(-\frac{1}{2}\chi^2_{\rm tot}\right), \quad \chi^2_{\rm tot} = \chi^2_{\rm SN} + \chi^2_{\rm CC} + \chi^2_{\rm GRB}. \tag{3.7}$$

and the likelihood is $\mathcal{L} \propto \exp(-\chi^2_{\rm tot}/2)$.

3.2 Model Selection: AIC and BIC

We quantified the relative performance of the models using the Akaike Information Criterion (AIC) and the Bayesian Information Criterion (BIC), defined as

$$\mathrm{AIC} = \chi^2_{\min} + 2k, \tag{3.8}$$

$$\mathrm{BIC} = \chi^2_{\min} + k \ln N, \tag{3.9}$$

where k is the number of free parameters and N is the total number of data points. Smaller values of AIC and BIC indicate a more favored model.

4 Results and Disscussion

The model parameters for Barrow Holographic Dark Energy (BHDE), Ricci Dark Energy (RDE), and New Agegraphic Dark Energy (NADE) were constrained using the combined cosmic chronometer (CC), gamma ray burst (GRB),and Type Ia supernova (SN) datasets. The resulting marginalized one and two dimensional probability distributions are shown in the corner plots, indicating 68% and 95% confidence contours. The best–fit values with 1σ uncertainties are summarized in Table 1, while Table 2 presents the corresponding model selection statistics.

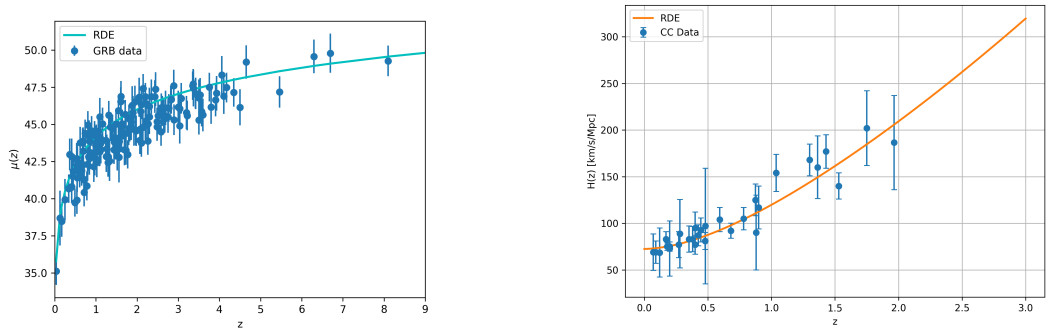

Figure 1: Comparison between the Ricci Dark Energy (RDE) model predictions and observational data. *Left:* The distance modulus $\mu(z)$ as a function of redshift, showing the RDE theoretical curve (solid line) against Gamma-Ray Burst (GRB) measurements with 1σ uncertainties. *Right:* The Hubble parameter $H(z)$ evolution compared with cosmic chronometer (CC) data.

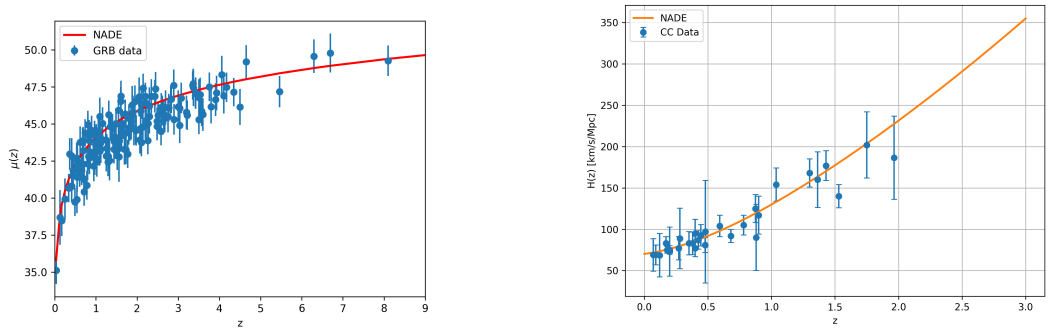

Figure 2: Comparison between the New Agegraphic Dark Energy (NADE) model predictions and observational data. *Left:* The distance modulus $\mu(z)$ as a function of redshift, showing the NADE theoretical curve (solid line) against Gamma-Ray Burst (GRB) measurements with 1σ uncertainties. *Right:* The Hubble parameter $H(z)$ evolution compared with cosmic chronometer (CC) data.

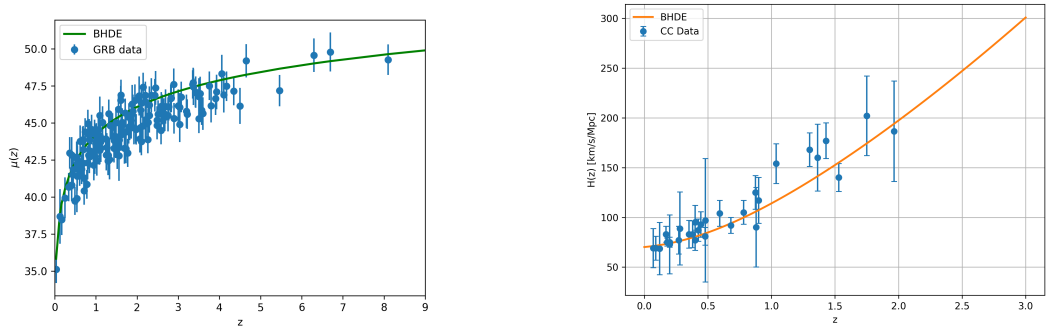

Figure 3: Comparison between the Barrow Holographic Dark Energy (BHDE) model predictions and observational data. *Left:* The distance modulus $\mu(z)$ as a function of redshift, showing the BHDE theoretical curve (solid line) against Gamma-Ray Burst (GRB) measurements with 1σ uncertainties. *Right:* The Hubble parameter $H(z)$ evolution compared with cosmic chronometer (CC) data.

Table 1: Best-fit values of the cosmological parameters for BHDE, RDE, and NADE models with 1σ uncertainties.

Model	H_0 [km s^{-1} Mpc^{-1}]	Ω_{m0}	Additional Parameter
BHDE	$69.76^{+0.135}_{-0.136}$	$0.301^{+0.0016}_{-0.0008}$	$\Delta = 0.9947^{+0.004}_{-0.0008}$
RDE	$72.428^{+0.346}_{-0.334}$	$0.302^{+0.022}_{-0.023}$	$\alpha = 0.398^{+0.029}_{-0.027}$
NADE	$70.165^{+8.443}_{-6.019}$	$0.399^{+0.049}_{-0.068}$	$n = 2.483^{+0.947}_{-0.561}$

Table 2: Model selection results based on the minimum $\chi^2_{\rm min}$, AIC and BIC for NADE,RDE and BHDE models.

Model	$\chi^2_{\rm min}$	**AIC**	**BIC**
NADE	600.703	604.703	614.613
RDE	600.728	604.728	614.638
BHDE	702.809	708.809	723.673

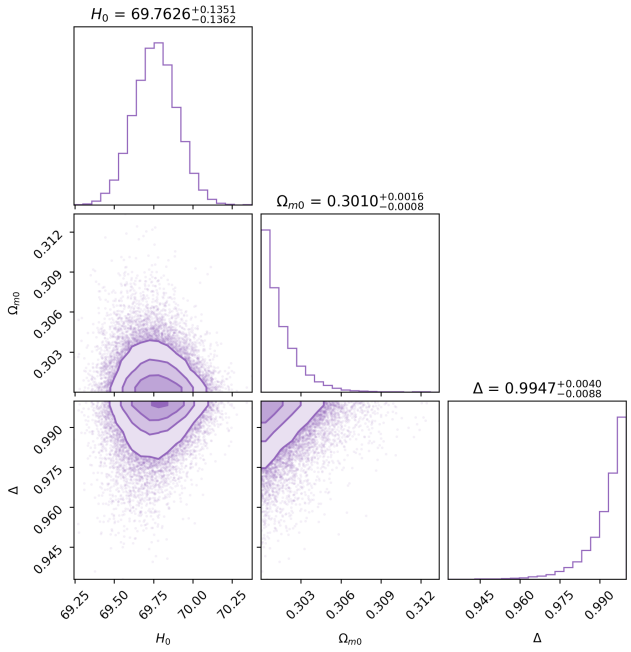

Figure 4: Corner plot for the BHDE model parameters constrained with CC + GRB + SN data. The diagonal plots show the marginalized one-dimensional distributions, while the off-diagonal plots show the joint 68% and 95% confidence regions.

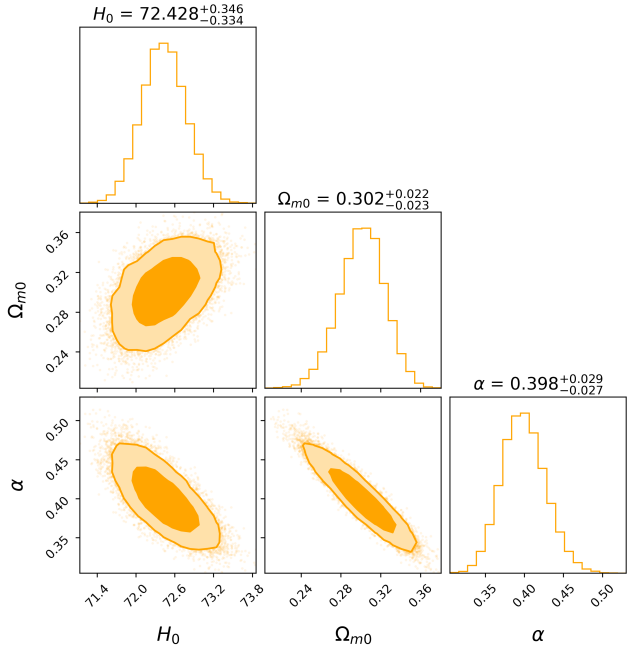

Figure 5: Corner plot for the RDE model parameters constrained with CC + GRB + SN data. The diagonal plots show the marginalized one-dimensional distributions, while the off-diagonal plots show the joint 68% and 95% confidence regions.

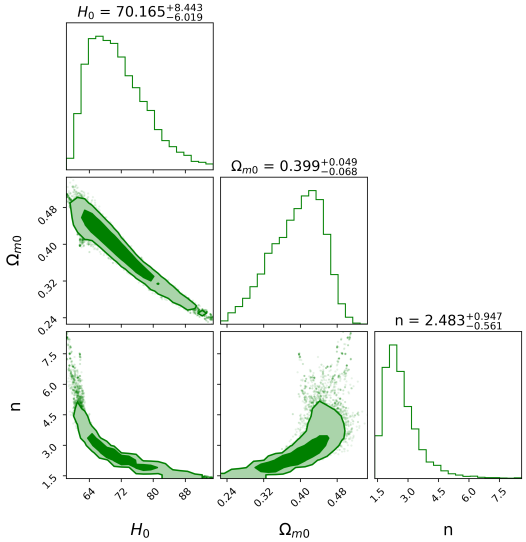

Figure 6: Corner plot for the NADE model parameters constrained with CC + GRB + SN data. The diagonal plots show the marginalized one-dimensional distributions, while the off-diagonal plots show the joint 68% and 95% confidence regions.

The Barrow holographic dark energy (BHDE) model modifies the standard holographic framework by introducing a deformation parameter Δ that captures possible quantum gravitational effects on the cosmic horizon entropy. In our present analysis, the joint CC + GRB + SNe Ia dataset yields

$$H_0 = 69.76^{+0.135}_{-0.136}\ \mathrm{km\,s^{-1}\,Mpc^{-1}}, \quad \Omega_{m0} = 0.301^{+0.0016}_{-0.0008}, \quad \Delta = 0.9947^{+0.004}_{-0.0008}.$$

These values point to a small but statistically significant deviation from the standard holographic case ($\Delta = 0$), implying a mild imprint of quantum geometry on the cosmic expansion. Earlier observational studies, such as those by Anagnostopoulos *et al.* [18], constrained the model using CC and SNe Ia data and obtained $\Delta = 0.095^{+0.093}_{-0.100}$ with $H_0 = 68.95^{+.0187}_{-0.0189}$ $\mathrm{km\,s^{-1}\,Mpc^{-1}}$

A more recent analysis by Luciano *et al.* [26], employing the SN+OHD+BAO combination from DESI DR2, reported $H_0 = 68.6^{+1.3}_{-3.3}\ \mathrm{km\,s^{-1}\,Mpc^{-1}}$, $\Omega_{m0} = 0.316^{+0.020}_{-0.023}$, and an upper limit $\Delta < 0.471$ (1σ). Compared to these works, our study finds a tighter constraint and a higher Δ value, reflecting the impact of incorporating high-redshift GRB data that improve sensitivity to the late-time expansion rate. Overall, the results suggest that the BHDE framework remains observationally consistent and capable of reproducing ΛCDM-like behavior with minor quantum corrections.

The Ricci dark energy (RDE) scenario connects the infrared cutoff to the Ricci scalar curvature, with the model evolution governed by the parameter α. Using the CC + GRB + SNe Ia dataset, the present analysis yields

$$H_0 = 72.428^{+0.346}_{-0.334}\ \mathrm{km\,s^{-1}\,Mpc^{-1}}, \quad \Omega_{m0} = 0.302^{+0.022}_{-0.023}, \quad \alpha = 0.398^{+0.029}_{-0.027}.$$

This slightly higher H_0 value compared with previous works indicates a faster late-time cosmic expansion, consistent with the addition of GRB data extending beyond $z \simeq 2$.

Earlier analyses, including those by Zhang [15], Xu *et al.* [27], and Xu and Wang [28], found $\alpha \simeq 0.36$–0.38, $\Omega_{m0} \approx 0.30$, and $H_0 \sim 69\ \mathrm{km\,s^{-1}\,Mpc^{-1}}$ based on lower-redshift SN, BAO,CMB and OHD datasets. The improved constraints obtained in the present work

demonstrate reduced parameter degeneracy and confirm the internal consistency of the RDE framework with modern data, while offering more precise cosmological limits compared to earlier efforts.

The new agegraphic dark energy (NADE) model refines the original agegraphic approach by relating the quantum energy density to the conformal time of the Universe, characterized by the parameter n. Our joint CC + GRB + SNe Ia analysis provides the following best-fit results:

$$H_0 = 70.165^{+8.443}_{-6.019}\ \mathrm{km\,s^{-1}\,Mpc^{-1}}, \quad \Omega_{m0} = 0.399^{+0.049}_{-0.068}, \quad n = 2.483^{+0.947}_{-0.561}.$$

The central value of n agrees well with previous estimates, which generally favor $n \approx 2.5$–2.8.

Wei and Cai [29] first analyzed the model using SNe Ia, CMB, and BAO data, obtaining $n = 2.716^{+0.111}_{-0.109}$ and $\Omega_{m0} = 0.295 \pm 0.020$. Zhang *et al.* [30] later extended the analysis to non-flat cosmologies and found $n = 2.673^{+0.053}_{-0.077}$, while Xu and Zhang [31] reported $n = 2.455$ with $\Omega_{m0} = 0.336$ and $h = 0.629$. The broader uncertainty in the present study is primarily due to the inclusion of GRB data, which introduces a mild degeneracy between H_0 and n. Nevertheless, the results reaffirm that $n \approx 2.5$ provides a viable description of the late-time acceleration, maintaining strong consistency with ΛCDM-like expansion while accommodating dynamical dark-energy behavior.

Table 3: Best-fit cosmological parameters for the BHDE, RDE, and NADE models compared with previous constraints from the literature. Errors represent 1σ uncertainties.

Model	Reference	Key Parameter	Ω_{m0}	H_0 ($\mathrm{km\,s^{-1}\,Mpc^{-1}}$)
BHDE	Anagnostopoulos *et al.* [18]	$\Delta = 0.095^{+0.093}_{-0.100}$	—	$68.95^{+0.0187}_{-0.0189}$
	Luciano *et al.* [26]	$\Delta < 0.471$	$0.316^{+0.020}_{-0.023}$	$68.6^{+1.3}_{-3.3}$
	This work (CC+GRB+SNe Ia)	$\mathbf{\Delta = 0.9947^{+0.004}_{-0.0008}}$	$\mathbf{0.301^{+0.0016}_{-0.0008}}$	$\mathbf{69.76^{+0.135}_{-0.136}}$
RDE	Zhang [15]	$\alpha = 0.359^{+0.024}_{-0.025}$	$0.318^{+0.026}_{-0.024}$	—
	Xu *et al.* [27]	$\alpha = 0.38 \pm 0.03$	0.34 ± 0.04	—
	Xu & Wang [28]	$\alpha = 0.382^{+0.033}_{-0.042}$	$0.2927^{+0.042}_{-0.032}$	$69.09^{+2.5}_{-2.3}$
	This work (CC+GRB+SNe Ia)	$\alpha = \mathbf{0.398^{+0.029}_{-0.027}}$	$\mathbf{0.302^{+0.022}_{-0.023}}$	$\mathbf{72.428^{+0.346}_{-0.334}}$
NADE	Wei & Cai [29]	$n = 2.716^{+0.111}_{-0.109}$	0.295 ± 0.020	—
	Zhang *et al.* [30]	$n = 2.673^{+0.053}_{-0.077}$	—	—
	Xu & Zhang [31]	$n = 2.455$	0.336	62.9
	This work (CC+GRB+SNe Ia)	$\mathbf{n = 2.483^{+0.947}_{-0.561}}$	$\mathbf{0.399^{+0.049}_{-0.068}}$	$\mathbf{70.165^{+8.443}_{-6.019}}$

The combined analysis of the BHDE, RDE, and NADE models using the joint CC+GRB+SNe Ia dataset provides a consistent and high-precision set of cosmological constraints. For the Barrow holographic model, the deformation parameter $\Delta = 0.9947^{+0.004}_{-0.0008}$ indicates a minute but physically meaningful deviation from standard holography, suggesting that the Barrow entropy framework can effectively encode quantum-gravitational imprints within cosmic evolution.The corresponding matter density $\Omega_{m0} = 0.301^{+0.0016}_{-0.0008}$ and expansion rate $H_0 = 69.76^{+0.135}_{-0.136}\,\mathrm{km\,s^{-1}\,Mpc^{-1}}$ remain consistent with Planck 2018 results[32], while slightly reducing the tension with late-universe measurements.

5 Conclusion

In this work, we performed a unified observational analysis of three prominent dynamical dark energy models Barrow Holographic Dark Energy (BHDE), Ricci Dark Energy (RDE), and New Agegraphic Dark Energy (NADE), using a combined dataset comprising cosmic chronometers (CC), gamma-ray bursts (GRBs), and type Ia supernovae (SNe Ia). This joint approach enables a consistent comparison of their cosmological behavior across both low and high redshifts.

The results indicate that all three models are broadly consistent with current observational bounds, yet each displays a distinct physical signature. The BHDE framework yields a deformation parameter $\Delta \simeq 1$, implying an almost standard holographic entropy with a subtle quantum gravitational correction. Its corresponding expansion rate, $H_0 \approx 69.8\,\mathrm{km\,s^{-1}\,Mpc^{-1}}$, is closely aligned with the Planck CMB determination [32], providing an intermediate value that alleviates the long-standing tension between early and late universe measurements without conflicting with the SH0ES [33] results.

The RDE model, characterized by the parameter $\alpha \approx 0.40$, predicts a slightly larger Hubble constant of $H_0 \approx 72.4\,\mathrm{km\,s^{-1}\,Mpc^{-1}}$, naturally trending toward the locally measured expansion rate. This behavior suggests that the RDE scenario may accommodate a faster cosmic acceleration, serving as a potential bridge between the Planck and SH0ES determinations of H_0.

Meanwhile, the NADE model provides a best-fit parameter $n \approx 2.5$ with moderate uncertainty, consistent with theoretical expectations from earlier studies. Its statistical preference, as reflected in lower AIC and BIC values, highlights its efficiency in reproducing the observed expansion history while preserving a physically motivated connection between quantum fluctuations and cosmic dynamics.

The inclusion of GRB data extends the redshift coverage beyond the reach of SNe Ia and CC probes, thereby tightening the constraints and mitigating degeneracies between model parameters. This integrated dataset strengthens the empirical foundation for testing holographic and agegraphic models of dark energy.

Overall, our comparative analysis demonstrates that modified holographic scenarios remain robust alternatives to the standard ΛCDM model. Among them, the BHDE formulation provides the most stable and tightly constrained results, reinforcing its potential as a theoretical link between quantum gravitational effects and late-time cosmic acceleration. Future work incorporating BAO, CMB, and forthcoming redshift drift observations will further refine these constraints and help clarify the role of entropy deformation and agegraphic corrections in resolving the current cosmological tensions.

Data Availability

The manuscript has no associated data or the data will not be deposited.

Conflicts of Interest

The author declares that there is no conflict of interest.

Ethical Considerations

The author has diligently addressed ethical concerns, including informed consent, plagiarism, data fabrication, misconduct, falsification, double publication, redundancy, submission, and other related matters.

Funding

This research did not receive any grant from funding agencies in the public, commercial, or non-profit sectors.

Acknowledgments

I am grateful to the anonymous referees for the constructive comments that helped enhance this manuscript and to my mother for her continuous encouragement and financial support.

References

[1] A. G. Riess, A. V. Filippenko, P. Challis, et al., "Observational evidence from supernovae for an accelerating universe and a cosmological constant," Astron. J. **116**, 1009 (1998). DOI: 10.1086/300499.

[2] S. Perlmutter, G. Aldering, G. Goldhaber, et al., "Measurements of Ω and Λ from 42 high-redshift supernovae," Astrophys. J. **517**, 565 (1999). DOI: 10.1086/307221.

[3] N. Aghanim, Y. Akrami, M. Ashdown, et al. (Planck Collaboration), "Planck 2018 results. VI. Cosmological parameters," Astron. Astrophys. **641**, A6 (2020). DOI: 10.1051/0004-6361/201833910.

[4] D. J. Eisenstein, I. Zehavi, D. W. Hogg, et al., "Detection of the baryon acoustic peak in the large-scale correlation function of SDSS luminous red galaxies," Astrophys. J. **633**, 560 (2005). DOI: 10.1086/466512.

[5] R. Jimenez and A. Loeb, "Constraining cosmological parameters based on relative galaxy ages," Astrophys. J. **573**, 37 (2002). DOI: 10.1086/340549.

[6] D. Scolnic, B. Popovic, A. Riess, et al., "The Pantheon+ analysis: Cosmological constraints," Astrophys. J. **938**, 113 (2022). DOI: 10.3847/1538-4357/ac8e04.

[7] S. Weinberg, "The cosmological constant problem," Rev. Mod. Phys. **61**, 1 (1989). DOI: 10.1103/RevModPhys.61.1.

[8] A. G. Cohen, D. B. Kaplan, and A. E. Nelson, "Effective field theory, black holes, and the cosmological constant," Phys. Rev. Lett. **82**, 4971 (1999). DOI: 10.1103/PhysRevLett.82.4971.

[9] G. 't Hooft, "Dimensional reduction in quantum gravity," arXiv:gr-qc/9310026, DOI: 10.48550/arXiv.gr-qc/9310026.

[10] L. Susskind, "The world as a hologram," J. Math. Phys. **36**, 6377 (1995). DOI: 10.1063/1.531249.

[11] M. Li, "A model of holographic dark energy," Phys. Lett. B **603**, 1 (2004). DOI: 10.1016/j.physletb.2004.10.014.

[12] C. Gao, F. Q. Wu, X. Chen, and Y. G. Shen, "A holographic dark energy model from Ricci scalar curvature," Phys. Rev. D **79**, 043511 (2009). DOI: 10.1103/PhysRevD.79.043511.

[13] H. Wei, R. G. Cai, "A new model of agegraphic dark energy," Phys. Lett. B **660**, 113 (2008). DOI: 10.1016/j.physletb.2007.12.030.

[14] J. D. Barrow, "The Area of a Rough Black Hole," Phys. Lett. B **808**, 135643 (2020), DOI: 10.1016/j.physletb.2020.135643.

[15] X. Zhang, "Holographic Ricci dark energy: Current observational constraints, quintom feature, and the reconstruction of scalar-field dark energy," Phys. Rev. D **79**, 103509 (2009). DOI: 10.1103/PhysRevD.79.103509.

[16] R. G. Cai, "A dark energy model characterized by the age of the universe," Phys. Lett. B **657**, 228 (2007). DOI: 10.1016/j.physletb.2007.09.061.

[17] E. N. Saridakis, "Barrow holographic dark energy," Phys. Rev. D **102**, 123525 (2020). DOI: 10.1103/PhysRevD.102.123525.

[18] F. K. Anagnostopoulos, S. Basilakos, E. N. Saridakis, "Observational constraints on Barrow holographic dark energy," Eur. Phys. J. C **80**, 826 (2020). DOI: https://doi.org/10.48550/arXiv.2005.10302.

[19] M. Moresco, L. Pozzetti, A. Cimatti, et al., "A 6% measurement of the Hubble parameter at $z \sim 0.45$: direct evidence of the epoch of cosmic re-acceleration," JCAP **05**, 014 (2016). DOI: 10.1088/1475-7516/2016/05/014.

[20] N. Liang, W. K. Xiao, Y. Liu and S. N. Zhang, "A Cosmology-Independent Calibration of Gamma-Ray Burst Luminosity Relations and the Hubble Diagram," Astrophysical Journal **685**, 354 (2008). DOI: https://doi.org/10.1086/590903.

[21] M. Demianski, E. Piedipalumbo, D. Sawant, and L. Amati, "Cosmology with gamma-ray bursts: I. The Hubble diagram through the calibrated $E_{p,i}$–$E_{\rm iso}$ correlation," Astronomy & Astrophysics **598**, A112 (2017). DOI: https://doi.org/10.1051/0004-6361/201628909.

[22] M. Demianski, E. Piedipalumbo, C. Rubano, and P. Scudellaro, "Cosmology with gamma-ray bursts. II. Cosmography challenges and cosmological scenarios," Astronomy & Astrophysics **598**, A113 (2017). DOI: 10.1051/0004-6361/201628911.

[23] S. Wang, Y. Wang, and M. Li, "Holographic dark energy," Phys. Rep. **696**, 1 (2017). DOI: 10.1016/j.physrep.2017.06.003.

[24] D. Stern, R. Jimenez, L. Verde, M. Kamionkowski, and S. A. Stanford, "Cosmic chronometers: constraining the equation of state of dark energy. I: H(z) measurements," JCAP **02**, 008 (2010). DOI: 10.1088/1475-7516/2010/02/008.

[25] D. M. Scolnic, D. O. Jones, A. Rest, et al., "The complete light-curve sample of spectroscopically confirmed SNe Ia from Pan-STARRS1 and cosmological constraints from the combined Pantheon sample," Astrophys. J. **859**, 101 (2018). DOI: 10.3847/1538-4357/aab9bb.

[26] G. G. Luciano, A. Paliathanasis, and E. N. Saridakis, "Constraints on Barrow and Tsallis holographic dark energy from DESI DR2 BAO data," JHEAP **49**, 100427 (2026). DOI: 10.1016/j.jheap.2025.100427.

[27] L. Xu, W. Li, J. Lu, B. Chang, "Cosmic constraint on Ricci dark energy model," Mod. Phys. Lett. A **24**, 1355 (2009). DOI: 10.1142/S0217732309028850.

[28] L. Xu and Y. Wang, "Observational constraints to Ricci dark energy model by using: SN, BAO, OHD, $f_{\rm gas}$ data sets," JCAP **06**, 002 (2010). DOI: 10.1088/1475-7516/2010/06/002

[29] H. Wei and R.-G. Cai, "Cosmological constraints on new agegraphic dark energy," Phys. Lett. B **663**, 1 (2008). DOI: 10.1016/j.physletb.2008.03.048.

[30] J.-F. Zhang, Y.-H. Li, and X. Zhang, "A global fit study on the new agegraphic dark energy model," Eur. Phys. J. C **73**, 2280 (2013). DOI: 10.1140/epjc/s10052-013-2280-6.

[31] Y.-Y. Xu and X. Zhang, "Comparison of dark energy models after Planck 2015," Eur. Phys. J. C **76**, 588 (2016), DOI: 10.1140/epjc/s10052-016-4446-5.

[32] N. Aghanim et al. (Planck Collaboration), "Planck 2018 results. VI. Cosmological parameters," Astronomy & Astrophysics **641**, A6 (2020). DOI: 10.1051/0004-6361/201833910.

[33] A. G. Riess, W. Yuan, L. Breuval, et al., "A Comprehensive Measurement of the Local Value of the Hubble Constant with 1 km s^{-1} Mpc^{-1} Uncertainty from the Hubble Space Telescope and the SH0ES Team," Astrophys. J. Lett. **934**, L7 (2022). DOI: 10.3847/2041-8213/ac5c5b.